Materials Advances

ROYAL SOCIETY OF CHEMISTRY

PAPER

View Article Online
View Journal | View Issue

Cite this: *Mater. Adv.*, 2025, 6, 5901

Hollow porous molecularly imprinted polymer for xylose detection in sugarcane bagasse by dispersive solid-phase extraction†

Diogo Hideki Moriya,[ab] Cláudio Fernando de Souza Teles,[ab] Paula Mantovani dos Santos,[ab] Ademar Wong[ab] and Maria D. P. T. Sotomayor *[ab]

The increasing generation of agro-industrial waste in Brazil presents an opportunity for the recovery of high value-added compounds. Xylose, a pentose derived from the hydrolysis of xylan, has several industrial applications, such as in the production of xylitol and furfural. In this study, a new xylose-selective hollow porous molecularly imprinted polymer (HMIP) was developed and applied to sugarcane samples *via* dispersive solid phase extraction (DSPE). The interaction occurred between the functional monomer and the template (xylose), followed by polymerization and subsequent removal of the template, creating selective cavities. The use of functionalized silica (SiO_2–C═C) as a core allowed the formation of hollow and porous structures, improving mass transfer and adsorption efficiency. The results indicated that the HMIP presented a maximum adsorption capacity of 22.99 mg g^{-1}, more than twice the capacity recorded for conventional MIPs. The polymer demonstrated high selectivity for xylose compared to other monosaccharides (glucose, arabinose, fructose, and sucrose), in addition to an adsorption efficiency of 83.80% in real samples of sugarcane bagasse hemicellulosic hydrolysate. In the solid phase removal (SPE) application, the HMIP reached 98.75% adsorption and maintained a high recovery rate after three reuse cycles (>93%). The results demonstrate the potential of the HMIP for the selective separation of xylose, contributing to the valorization of agro-industrial waste and promoting safe practices aligned with the principles of the circular economy and SDG 12 (responsible consumption and production).

Received 15th May 2025,
Accepted 6th July 2025

DOI: 10.1039/d5ma00493d

rsc.li/materials-advances

1. Introduction

The increasing generation of agro-industrial waste has driven the search for sustainable strategies to use these byproducts. In Brazil, the sugar-energy sector stands out as one of the pillars of the economy, generating large quantities of residual biomass, such as bagasse, straw and filter cake, which are often discarded without adequate treatment. One of the main components of this waste is hemicellulose, a heterogeneous polysaccharide rich in xylan. When subjected to acid hydrolysis, xylan is converted into xylose, a high-value monosaccharide used in the production of compounds such as xylitol and furfural.[1]

The selective extraction of xylose from complex matrices represents an analytical challenge, due to the presence of interferents such as other monosaccharides and biomass-derived compounds.[2] Traditional separation methods, such as liquid–liquid extraction and chromatography, often require multiple steps, expensive reagents, and large volumes of solvents, making them inefficient and unsustainable.[3] In this context, molecularly imprinted polymers (MIPs) emerge as a promising alternative, capable of selectively recognizing and adsorbing xylose even in the presence of interferents.[4]

In recent years (2022–2024), several studies have reported the use of MIPs for the separation and detection of sugars, especially glucose, fructose, and xylitol. However, most of these studies still focus on conventional solid MIPs or core@shell systems, which, although presenting advances in selectivity, continue to be limited by the low accessibility of recognition sites, restricted analyte diffusion, and lower reusability. In addition, many of these synthesis processes use unsustainable routes, with high consumption of organic solvents and toxic reagents, hindering their industrial scalability.[5–8]

Among the recent approaches for the synthesis of molecularly imprinted polymers (MIPs), hollow porous materials (HMIPs) stand out for presenting a differentiated structural

[a] *São Paulo State University (UNESP), Institute of Chemistry, Araraquara, SP, Brazil. E-mail: m.sotomayor@unesp.br*
[b] *National Institute for Alternative Technologies of Detection, Toxicological Evaluation and Removal of Micropollutants and Radioactives (INCT-DATREM), 14801-970, Araraquara, São Paulo, Brazil*

† Electronic supplementary information (ESI) available. See DOI: https://doi.org/10.1039/d5ma00493d

architecture, capable of overcoming limitations associated with mass transfer observed in conventional MIPs. This structure, composed of thin and highly porous walls, promotes greater accessibility to recognition sites, favoring the diffusion of the analyte and, consequently, increasing both the adsorption capacity and the selectivity of the material.[8] The synthesis of HMIPs is generally based on the use of functionalized silica cores as temporary molds for the formation of the polymer layer. After the polymerization step, the silica core is removed, resulting in a polymer with accessible cavities both on the surface and in the internal region of the porous wall. This three-dimensional configuration maximizes the specific surface area, increases the number of available active sites and significantly improves the efficiency of interactions with the target analyte, especially in fast and selective adsorption processes.

Recent studies have demonstrated the benefits of this architecture. For example, HMIPs developed for tetracycline (2022) showed a two- to three-fold larger surface area and equally superior adsorption capacity when compared to traditional MIPs and core@shell systems, achieving recovery rates between 74% and 96%.[9] Similarly, in 2022, a magnetic HMIP based on MOFs for ciprofloxacin extraction was reported, which achieved adsorption capacity close to 75 mg g^{-1}, with high selectivity and reduced equilibrium time to approximately 50 minutes.[10] More recent reviews (2023–2024) confirm that HMIPs offer superior kinetic performance, attributed to improved analyte diffusion, in addition to presenting higher adsorption efficiency compared to conventional MIPs.[11]

Although the application of HMIPs has been mainly focused on the capture of pharmaceuticals, pesticides and environmental contaminants, there has been a growth in the development of materials aimed at the separation of sugars, such as glucose and fructose.[12] Classical studies have already explored macroporous MIPs using monomers containing boronic groups for the selective recognition of carbohydrates. However, recent studies reinforce that the adoption of porous surfaces is essential to improve the accessibility of recognition sites and, consequently, the selectivity and capture capacity of monosaccharides.[8,11,12] Even so, gaps remain in the literature regarding the application of HMIPs for xylose, especially in complex matrices originating from lignocellulosic residues.

Another relevant aspect is that, although some of the recent HMIPs are developed using synthetic routes considered more sustainable—with reduced use of toxic organosolvents and fewer steps—there are still significant challenges, such as structural fragility of the hollow walls and limitations on the long-term reuse of the materials.[9] More recent research has sought to overcome these limitations, proposing functionalized HMIPs with photo- and heat-sensitive responses, in addition to improvements in mechanical robustness. However, such advances have not yet been specifically aimed at the selective extraction of sugars from agro-industrial waste. In this scenario, the present study stands out for developing, for the first time, a selective HMIP for xylose, using as a functional matrix a derivative of sugarcane bagasse, an abundant waste from the Brazilian sugar and ethanol industry. Unlike previous studies, which generally focused on conventional MIPs, the adoption of the hollow porous architecture in this work resulted in significant gains in adsorption capacity, selectivity, and kinetics, even under challenging conditions with high loads of interferents.[13] In addition, the adopted synthetic strategy prioritizes green chemistry principles, with a significant reduction in the use of toxic solvents, recycling of reagents, and minimal waste generation. The structural robustness of the developed material allowed its repeated use, without significant loss of performance, overcoming challenges frequently reported in the literature regarding the durability of HMIPs.

The integration of the polymer into the dispersive solid-phase extraction technique (HMIP-DSPE) represents an advance not only from an analytical point of view, but also from an economic and environmental point of view, as it simplifies sample preparation, reduces solvent consumption, and increases the scalability of the process, making it applicable in industrial contexts focused on the valorization of lignocellulosic waste. Dispersive solid phase extraction (DSPE) is a widely used technique for sample preparation in chemical analysis, as it allows the rapid and selective separation of analytes in complex matrices.[14] The incorporation of MIPs in DSPE (MIP-DSPE) represents an effective strategy for the selective extraction of xylose, reducing interferents and improving the accuracy of analyses. Furthermore, the use of MIPs in reusable systems, such as solid phase extraction (SPE), can increase the economic and environmental viability of the technique, favoring its large-scale application.

Despite advances in the development of MIPs for various analytes, few studies address their application in the selective extraction of xylose, and even fewer explore the use of hollow porous MIPs for this purpose. Therefore, this work aimed to develop a hollow porous molecularly imprinted polymer consistently selective for xylose, evaluating its efficiency in the extraction and purification of this monosaccharide from agro-industrial waste. The characterization of the material, the optimization of the extraction conditions and its application in real samples were central aspects of this study, which seeks to contribute to the sustainable use of waste and the development of innovative materials for chemical analysis.

2. Materials and methods

2.1. Reagents and solutions

Solutions were prepared using standard HPLC or analytical grade chemical reagents and ultrapure water from the Milli-Q® system with a resistivity of 18.2 MΩ cm. To avoid contamination, all glassware was pretreated according to appropriate laboratory protocols.

For the synthesis of hollow porous molecularly imprinted polymers (HMIPs and HNIPs), reagents were purchased from Sigma-Aldrich®, including D-xylose (purity ≥99%), acrylamide (ACR, purity ≥99%), *N*,*N*′-methylenebisacrylamide (MBAm, purity ≥99%), and azobisisobutyronitrile (AIBN, purity ≥99%). Hollow porous synthesis was performed using sodium hydroxide

(NaOH) and concentrated hydrofluoric acid (HF), both from Sigma-Aldrich®. Silica nanoparticles were synthesized using tetraethylorthosilicate (TEOS, purity ≥99%) and γ-methacryloxypropyltrimethoxysilane (γ-MPS, purity ≥99%), both from Sigma-Aldrich®.

The interference and selectivity studies were conducted using D-arabinose, D-fructose, D-glucose and D-sucrose, all purchased from Sigma-Aldrich®. The solvents used in different stages of the study included acetonitrile (ACN), hydrochloric acid (HCl, 37%), ethanol, dimethyl sulfoxide (DMSO), ammonium hydroxide (NH_4OH, 28%) and acetic acid (HAc), all obtained from Synth®. For the spectrophotometric determination of xylose, phloroglucinol (purity ≥99%) from Sigma-Aldrich® was used.

2.2. Apparatus

The experiments were conducted using specific equipment for temperature control, separation and analysis of the polymers. Temperature control during polymer synthesis and washing procedures in the Soxhlet system was performed with the aid of a SOLAB Científica® digital ultra-thermostatic bath (model SL-152I), operating in the temperature range of −10 °C to 100 °C, with a resolution of ±0.1 °C and an accuracy of up to 0.5 °C. The system has a U resistance of 1200 W and a power supply of 220 V. Spectrophotometric analysis was performed on an Agilent Technologies® UV-Vis spectrophotometer (Cary 60 model). Quartz cuvettes with a 1.0 cm optical path were used to record measurements in solutions, in the spectral range from 200 to 800 nm.

The polymer washing steps were carried out using FISATOM® thermal blankets (model 12E), with a capacity of 125 mL and a power of 80 W (220 V). The separation of polymers from solutions during the adsorption tests was performed using a Centrilab® centrifuge (model 80-2B-15 mL), with a maximum speed of 4000 rpm and a relative centrifugal force of 2.325 × *g* (power supply 100–240 V). The filtration processes were carried out in a Büchner funnel coupled to a kitasato flask and a Prismatic® vacuum pump (model 121 Type 2 VC), oil-free and powered at 220 V. The homogenization of the samples was performed in tubes with caps using a Nortecientífica® homogenizer (model NH-2200), with an electric motor with adjustable speed between 6 and 30 rpm and capacity for 40 tubes (110–220 V). All aqueous solutions were prepared using ultrapure water obtained from a Milli-Q® Ultra-Pure Water System (Millipore®, resistivity of 18.2 MΩ cm, 220 V).

Infrared spectra were recorded in a MB-100 Fourier-transform spectrometer operating in transmission mode (4000–400 cm^{-1}; conventional KBr pellet method) (Shimadzu, Japan). The polymers were characterized using different instrumental techniques. The morphology of the materials was analyzed by scanning electron microscopy (SEM) on a JEOL® model JSM-6610LV equipment, operating with adjustable acceleration voltage. The textural parameters of the polymers, such as specific surface area (SBET), total pore volume (VTP), and mean pore diameter (DMP), were calculated using adsorption–desorption isotherms with nitrogen gas at 77 K (−196 °C) and with relative tension between $\sim 10^{-6}$ and 0.995 mmHg, using the Quantachrome® Nova 1200e equipment coupled to an automatic gas analyzer (allQuantachrome, Boynton Beach, FL, USA).

The initial step for the quantification of D-xylose extracted from sugarcane straw and bagasse consisted of characterization of the hemicellulosic hydrolysate obtained from these biomasses. For this purpose, high-performance liquid chromatography with a refractive index detector (HPLC-RID) was used. The samples were previously filtered through 0.22 μm membranes before injection into the chromatographic system to remove suspended particles. The separation of monosaccharides was performed on a C18 column, maintained at 85 °C, using ultrapure water as the mobile phase in isocratic flow, with a flow rate of 0.6 mL min^{-1}. The injection volume was 20 μL. Detection was performed by refractive index detection, which is sensitive to non-volatile compounds such as sugars.

2.3. Synthesis of the HMIP and HNIP, sustainability evaluation and E-factor calculation

The synthesis of the porous hollow molecularly imprinted porous polymer (HMIP) was carried out in four main steps. Initially, silica nanoparticles were synthesized using 4.0 mL of tetraethylorthosilicate (TEOS) and functionalized with 1.0 mL of γ-methacryloxypropyltrimethoxysilane (γ-MPS) in a solution containing 30.0 mL of ethanol, 2.0 mL of NH_4OH (28%) and 8.0 mL of deionized water. After nanoparticle formation, molecularly imprinted polymerization was conducted by mixing 0.4 mmol of D-xylose (template molecule), 4.0 mmol of acrylamide (ACR) as a functional monomer, 20.0 mmol of *N*,*N*′-methylenebisacrylamide (MBAm) as a crosslinking agent and 1.0 mmol of azobisisobutyronitrile (AIBN) as a radical initiator in 50.0 mL of acetonitrile (ACN). The reaction was carried out under a nitrogen atmosphere at 60 °C for 24 h.

After polymer formation, the removal of the silica core was performed in two sequential steps, using specific corrosive agents. Initially, the materials were treated with a 2.0 mol L^{-1} NaOH solution under magnetic stirring, at room temperature (25 °C) for 12 hours, promoting partial solubilization of the silica by breaking the siloxane bonds (Si–O–Si). Subsequently, to ensure complete removal of the core, further treatment with 10% (v/v) concentrated hydrofluoric acid (HF) was performed, under strict safety conditions, in an exhaust hood and using personal protective equipment. This step was also conducted at room temperature, with a reaction time of 6 hours, ensuring the complete dissolution of the silica residues present in the structure.

The environmental impact of HMIP synthesis was assessed using the *E*-factor (environmental factor), a widely accepted metric in green chemistry that relates the total mass of waste generated to the mass of the final product.[15] The *E*-factor was calculated according to the following equation:

$$E = \frac{\text{Mass of total waste (kg)}}{\text{Mass of final product (kg)}} \quad (1)$$

The waste mass includes all solvents (acetonitrile, ethanol, water) used during the polymerization, purification (Soxhlet extraction), and template removal steps, as well as auxiliary reagents such as sodium hydroxide and hydrofluoric acid used for silica core removal. The mass of reagents incorporated into the final polymer structure (*e.g.*, monomers and crosslinkers) was not considered waste. Energy inputs were considered qualitatively based on reaction conditions (reaction time, temperature, and use of heating or stirring), but were not directly converted to quantitative energy metrics. However, the reduced reaction volume and shorter purification steps were key factors in minimizing energy consumption compared to conventional MIP synthesis.

For comparison, the conventional MIP synthesis route was modeled based on literature data, typically involving bulk or core@shell MIPs synthesized with larger solvent volumes and extended purification times (24–48 h). The estimated *E*-factor for HMIP synthesis was 230 kg of waste per kg of product, representing a 35% reduction compared to 350 kg kg^{-1} estimated for conventional MIPs under similar laboratory-scale conditions.

This estimate demonstrates the improved environmental profile of HMIP synthesis, contributing to more sustainable material production practices aligned with SDG 12 (responsible consumption and production).

2.4. D-Xylose quantification with phloroglucinol

D-Xylose quantification was performed using the spectrophotometric method described by Borges *et al.*, using phloroglucinol as a colorimetric reagent.[5] To prepare the reagent, 0.5 g of phloroglucinol (>99.0%) was dissolved in 100.0 mL of glacial acetic acid (>99.7%), with subsequent addition of 10.0 mL of hydrochloric acid (37%). A 0.4 mL aliquot of the sample containing D-xylose was then mixed with 1.6 mL of the phloroglucinol solution in a sealed tube, and the mixture was heated in a boiling water bath for 10 minutes. After this period, the tube was cooled to room temperature for 5 minutes, and the absorbance of the solution was determined using an UV-Vis spectrophotometer. The use of phloroglucinol as a colorimetric reagent is justified by its high reactivity with pentoses in a strongly acidic medium, resulting in the formation of stable-colored compounds that can be detected by spectrophotometry. In this condition, D-xylose undergoes dehydration, producing furfural, which reacts with phloroglucinol to form a product with an intense pink to red color. The intensity of the color generated is proportional to the concentration of D-xylose and it can be quantified by absorbance, generally measured in the range from 540 to 550 nm. This method stands out for the selectivity of phloroglucinol for pentoses, such as D-xylose, compared to hexoses, such as glucose, which makes it particularly useful in the analysis of lignocellulosic hydrolysates and other complex systems where selective quantification of xylose is desired. Furthermore, it is a sensitive, low-cost and easy-to-perform technique, widely used in biomass hydrolysis studies and in the monitoring of reducing sugars.[16–18]

2.5. Evaluation of HMIP reusability

Under optimized conditions, SPE was performed using 150 mg of HMIP/HNIP in 5 mL commercial cartridges containing polyethylene discs to retain the material. The system was conditioned with 5 mL of a mixture of acetonitrile and water (50 : 50, v/v) at 1 mL min^{-1}, followed by percolation of 5 mL of the sample (50 mg L^{-1} of xylose in acetonitrile) at 0.2 mL min^{-1}. Xylose was eluted with 5 mL of a water : ethanol solution at 0.5 mL min^{-1} and subsequently quantified by UV-Vis spectrophotometry using phloroglucinol. DSPE was performed under optimized sample mass and volume conditions, in a dispersive manner, with centrifugation steps for adsorbent separation.

The extraction parameters optimized in this study include adsorbent mass, solvent type for conditioning and elution, and contact time. The optimization was performed by systematically varying each variable, followed by the analysis of the xylose recovery efficiency. The amount of polymer used was adjusted between 50 and 200 mg, while different solvents and their proportions were tested to determine the best conditioning and elution conditions. The contact time was optimized by controlling the sample and elution flow rates, aiming to maximize adsorption and minimize losses during the process. The reusability of the cartridges was demonstrated in three consecutive DSPE cycles to verify polymer stability.

2.6. Study of adsorption kinetics and isotherm

The kinetic study was conducted to evaluate the dynamics of xylose adsorption on the synthesized polymers over time and to identify the kinetic model that best describes the process. For this purpose, a xylose solution with a fixed concentration of 50 mg L^{-1} was prepared and added to 13 mg of HMIP and HNIP. The interactions occurred under controlled agitation, and samples were collected at specific time intervals (5 to 120 minutes). After each period, the polymers were separated from the solution by centrifugation, and the residual xylose concentration was determined by UV-Vis spectrophotometry. From the data obtained, the equilibrium adsorption capacity (Q_e) was calculated according to eqn (2), adjusting the results to the pseudo-first order and pseudo-second order kinetic models.

$$Q_e = \frac{(C_0 - C_e) \times V}{m} \quad (2)$$

where C_0 is the initial xylose concentration (mg L^{-1}), C_e is the concentration (mg L^{-1}) of xylose at equilibrium, V is the volume of solution (L) and m is the adsorbent mass (g).

The adsorption isotherm study was performed to evaluate the maximum adsorption capacity of the HMIP and HNIP at different analyte concentrations, in addition to understanding the behavior of the interaction between the polymer and xylose. For this purpose, solutions containing xylose at varying concentrations (5 to 100 mg L^{-1}) were prepared and subjected to interaction with 13 mg of the polymers under constant stirring for 30 minutes, a time previously determined as sufficient for the equilibrium of the system. After adsorption, the polymers were separated from the solution by centrifugation and the

remaining xylose concentration was quantified by UV-Vis spectrophotometry. The equilibrium adsorption capacity (Q_e) was calculated using eqn (1). The experimental data were fitted to the adsorption linear isotherm models (Langmuir, Freundlich, Scatchard and Dubinin–Radushkevich) to determine the best mathematical description of the process. The Langmuir model assumes the formation of a homogeneous adsorption monolayer at the selective sites of the polymer, while the Freundlich model considers adsorption in multiple layers, with sites of varying energy. The coefficient of determination (R^2) was used to evaluate which model best represented the results obtained.

2.7. Study of selectivity and interferents

The selectivity test was performed to evaluate the affinity of the HMIP for xylose in relation to other monosaccharides that may be present in real samples. For this purpose, the polymers were homogenized separately in solutions containing 50 mg L^{-1} of xylose, arabinose, fructose, glucose and sucrose, and the adsorption capacity of each of the sugars by the polymers was analyzed. The interference test was conducted using binary mixtures of D-xylose/D-glucose, D-xylose/D-fructose and D-xylose/D-sucrose, all at a concentration of 50 mg L^{-1}, to verify whether the presence of other sugars affected the selective adsorption of the HMIP. The tests were performed in triplicate, with 30 minutes of interaction between the polymers and the prepared solutions.

The selection of the interferents was based on their structural similarity to xylose and the presence of these molecules in real samples, such as hemicellulosic hydrolysates. D-Glucose, D-fructose, and D-sucrose were chosen for their structural similarity to the target analyte and their common occurrence in plant biomass sugar mixtures. These molecules have hydroxyl groups (–OH) that can compete for the adsorption sites of the HMIP, especially in solutions containing multiple sugars. The analysis of these interferents was essential to evaluate the selective efficiency of the HMIP and its applicability in complex matrices.

The analytical standards used in all adsorption, selectivity and interference studies were certified analytical grade sugars (D-xylose, D-glucose, D-fructose, D-arabinose and sucrose) obtained from Sigma-Aldrich® (purity ≥99%).

2.8. Preparation of real samples

The preparation of real samples was carried out with the objective of applying the polymeric material in complex matrices and evaluating its efficiency in the selective extraction of xylose. The sugarcane bagasse samples were provided by the Applied Microbiology Group for Bioprocesses – IQ Unesp, Araraquara, SP, while the hydrolysate was obtained from straw and bagasse purchased from the Santa Cruz São Martinho sugar and alcohol plant, Américo Brasiliense, SP. The pretreatment consisted of acid hydrolysis, carried out at the National Center for Research in Energy and Materials (CNPEM), at the National Laboratory of Science and Technology of Bioethanol (CTBE), Campinas – SP, in a 250 L reactor operating at 140 °C, with 0.5% sulfuric acid (m/v) and a solid–liquid ratio of 1 : 10 for 15 minutes. After hydrolysis, the hydrolysate was filtered to separate the solid fraction and stored at 4 °C for later analysis using the method developed in this study. The orange pomace sample was obtained from fruits purchased at a local market in Araraquara, SP, and subjected to acid hydrolysis according to the National Renewable Energy Laboratory (NREL) protocol.

2.9. HPLC-RI analysis

High performance liquid chromatography with refractive index (HPLC-RI) analysis was performed to quantify the sugars present in the samples. Prior to analysis, the samples obtained from the biomass hydrolysis step were previously filtered in Sep-Pak C18 6 cc, 55–105 μm cartridges (Waters) to remove interfering compounds. Then, the solutions (20 μL) were injected into the Shimadzu HPLC system, equipped with a refractive index (RI) detector. The separation of the sugars glucose, xylose, and arabinose, as well as acetic acid, was performed using a mobile phase of 0.01 N H_2SO_4 in a BIO-RAD AMINEX HPX-87H analytical column (300 × 7.8 mm), maintained at 60 °C, with a flow rate of 0.6 mL min^{-1}.

3. Results and discussion

3.1. Polymer characterization

The FT-IR spectrum presented (Fig. 1) shows the characterization of different polymeric materials, including HMIP, HNIP, MIP core@shell (core–shell imprinted polymer), NIP core@shell (core–shell unimprinted polymer) and functionalized silica. The spectroscopic analysis allows the identification of the main chemical bonds present in the materials and the evaluation of the efficiency of functionalization and polymerization. The absorption bands detected suggest the presence of functional groups specific to each material. A carbonyl stretching band (C═O) is observed at approximately 1644 cm^{-1}, associated with the amide group of acrylamide. This signal presents small changes in intensity and position when comparing the HMIP and HNIP spectra, indicating the occurrence of

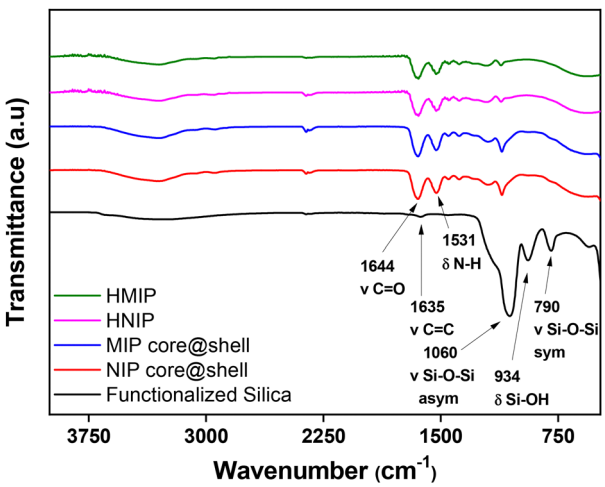

Fig. 1 FT-IR spectra of the synthesized materials: HMIP, HNIP, MIP core@shell, NIP core@shell and functionalized silica.

interactions, such as hydrogen bonds, between the hydroxyl groups of xylose and the amide groups of the monomer in the pre-polymerization stage.[6,19] The band at 1635 cm^{-1} is attributed to the C=C vibration, indicating the presence of bonds characteristic of the cross-linked polymer structure.[8,20] Furthermore, the absorption at 1531 cm^{-1} attributed to N–H deformation reinforces the presence of these intermolecular interactions, characteristic of the complexes formed before polymerization.[21,22] The changes in the bands and their variations are compatible with the formation of non-covalent interactions, predominantly hydrogen bonds, between xylose and acrylamide. This behavior is typical of MIP systems and is essential for the formation of selective sites in the final material. The bands at 1060 cm^{-1} and 964 cm^{-1} are attributed to the asymmetric vibration of Si–O–Si and the Si–OH vibration, respectively, confirming the presence of functionalized silica in the polymer matrix. The absence of silica in the HMIP/HNIP after NaOH/HF treatment, as confirmed by FTIR analysis, supports the successful removal of the silica core, thus validating the formation of the hollow structure characteristic of the porous imprinted polymer. The band at 790 cm^{-1} is attributed to the symmetric vibration of Si–O–Si, which reinforces the incorporation of silica in the synthesized polymers.[3,7,23,24] The comparison between the spectra of the different materials allows the evaluation of the structural modifications between the MIPs and NIPs. The presence of the analyte during the synthesis of MIPs can influence the molecular organization and chemical interactions, resulting in small variations in the intensities and displacements of the bands. Furthermore, the analysis of functionalized silica confirms its incorporation into polymers, indicating the success of the chemical modification.

The textural parameters obtained (Table 1) confirm the influence of the removal of the silica core on the structure of the materials. It is observed that the polymers in the hollow porous configuration (HMIP and HNIP) showed a significant increase in the specific surface area, with values of 124.30 m^2 g^{-1} for the HMIP and 114.30 m^2 g^{-1} for the HNIP, when compared to the core@shell materials (87.63 m^2 g^{-1} for the MIP and 63.82 m^2 g^{-1} for the NIP). This increase is directly associated with the generation of a hollow and highly porous structure after the removal of the silica mold, which provides greater exposure of the active sites and favors the diffusion of the analyte. The pore volume also showed a significant increase, going from 0.18 cm^3 g^{-1} (MIP) and 0.14 cm^3 g^{-1} (NIP) to 0.28 cm^3 g^{-1} (HMIP) and 0.20 cm^3 g^{-1} (HNIP). As for the average pore diameter, a slight expansion was observed after the removal of the core, ranging from approximately 3.16–3.17 nm in the core@shell materials to 3.75–3.77 nm in the hollow polymers. These data corroborate the SEM micrographs (Fig. 2), which evidence the formation of hollow structures, with thin and highly porous walls, confirming the effective elimination of the silica core. Improvements in textural parameters are fundamental to justifying the increase in adsorption capacity, selectivity and kinetics observed for the HMIP, since they favor accessibility and transport of the analyte to molecular recognition sites.

Table 1 Textural parameters obtained for MIP core@shell, NIP core@shell, HMIP (with template), HMIP, and HNIP

Polymers	Specific area (m^2 g^{-1})	Pore volume (cm^3 g^{-1})	Pore diameter (nm)
MIP core@shell (with template)	87.63	0.18	3.17
NIP core@shell	63.82	0.14	3.16
HMIP (with template)	101.50	0.19	3.75
HMIP	124.30	0.28	3.77
HNIP	114.30	0.20	3.75

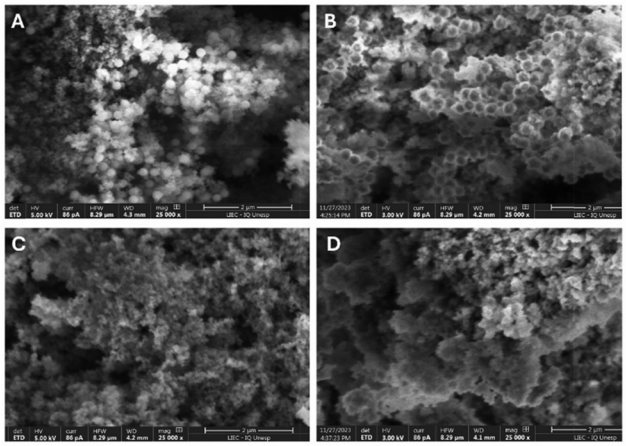

Fig. 2 Scanning electron microscopy (SEM) images showing the surface morphologies of the polymers: (A) SiO_2@–C=C@MIP, (B) SiO_2@–C=C@NIP, (C) HMIP, and (D) HNIP.

The SEM images (Fig. 2) reveal distinct structural differences between the analyzed materials. In image A (SiO_2@–C=C@MIP), well-defined and agglomerated particles are observed, indicating a homogeneous and porous coating due to the presence of the printed polymer layer. In general, MIPs present greater organization and well-defined porosity, while NIPs exhibit a less ordered and less defined structure, and hollow porous materials have a hollow architecture that may favor the adsorption of analytes. Image 2B (SiO_2@–C=C@NIP) shows a similar morphology to image A but with a less organized and homogeneous structure. In image 2C (HMIP), a highly porous and less dense structure is observed, indicating the efficient removal of the silica core and the formation of a material with high surface area and exposed recognition sites. In contrast, image 2D (hollow porous NIP) presents a more collapsed structure with less defined porosity, suggesting that the absence of molecular imprinting compromises structural stability. Overall, the efficiency of core removal was confirmed by the images, as they clearly show the structural transformation between the core@shell material and the hollow porous polymer. The absence of any solid residue in the core is observed, evidenced by the formation of hollow structures with thin and highly porous walls, characteristic of the complete elimination of silica. Comparatively, the materials before removal present spherical and dense morphology, while after treatment with NaOH and HF, the micrographs reveal well-defined internal

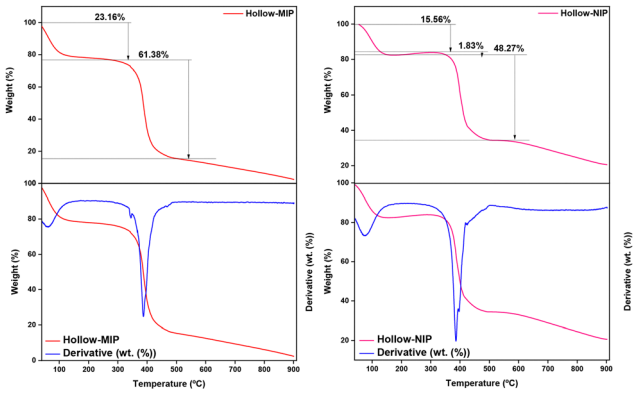

Fig. 3 TGA analysis of HMIP and HNIP: hollow-MIP (red line) and derivative (blue line).

cavities, confirming the success of obtaining the hollow porous architecture.

TGA analysis (Fig. 3) demonstrated that Hollow-MIP and Hollow-NIP exhibited two main mass loss events. The first event, occurring between 100 and 200 °C, is attributed to the evaporation of water and physically adsorbed volatiles. The second major loss, observed between 250 and 450 °C, corresponds to the decomposition of the organic polymer matrix. Hollow-MIP presented a higher total mass loss (84.54%) compared to Hollow-NIP (65.66%), confirming the greater amount of polymeric material in the imprinted structure. The residual mass, approximately 15% for Hollow-MIP and 34% for Hollow-NIP, is attributed to non-volatile carbonaceous residues rather than silica, as the core material was removed during synthesis. The derivative curves (DTG) also revealed distinct degradation profiles, with Hollow-MIP presenting broader peaks, indicative of more complex molecular interactions promoted by the imprinting process.

3.2. Optimization of parameters that influence DSPE and reusability

The determination of the ideal solvent for polymer adsorption was performed by comparing the efficiency of the material in different media. The results (Fig. 4A) indicated that adsorption was more efficient in solvents with lower water content. Several proportions of acetonitrile (ACN) and water (50 : 50, 75 : 25, 90 : 10, and 99 : 1, v/v) were tested, and an increase in xylose adsorption was observed with increasing ACN concentration. The 99 : 1 ACN : H_2O (v/v) system presented the best performance, as it minimized xylose solvation and favored its interaction with the selective cavities of the HMIP. Additional tests with other solvents, such as ethanol and dimethyl sulfoxide (DMSO), did not produce satisfactory results. Thus, the ACN : H_2O (99 : 1) system was selected for subsequent experiments, ensuring greater efficiency in analyte adsorption.

The results of the mass test (Fig. 4B) demonstrated that the adsorption of xylose by the polymer increased as the amount of polymer material was increased, until reaching a saturation point. Different polymer masses, ranging from 2 mg to 15 mg, were tested using a 50 mg L^{-1} xylose solution. From 13 mg of polymer, the adsorption stabilized, indicating that a greater amount of material would not result in a significant increase in adsorption. Additionally, the HMIP demonstrated a higher adsorption rate compared to the HNIP, indicating the selectivity of the HMIP for xylose. Based on these results, 13 mg was the mass chosen for the subsequent experiments, ensuring the best adsorption efficiency without wasting material.

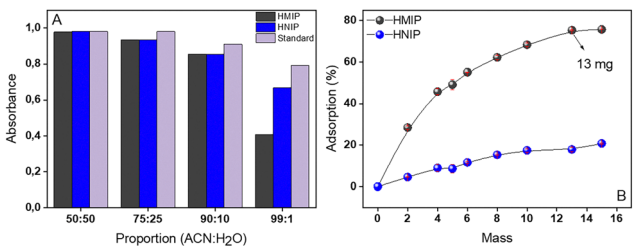

Fig. 4 Optimization of parameters that influence the DSPE analytical procedure. (A) optimization of solvent proportion; (B) optimization of HMIP and HNIP mass. n = 3.

3.3. Study of adsorption kinetics and isotherm

The results of the kinetic study demonstrated that the adsorption of xylose by the HMIP occurs rapidly, reaching equilibrium in approximately 30 minutes (Fig. 5). The adsorption capacity increased significantly in the first few minutes, stabilizing after this time, reaching a maximum adsorption capacity of approximately 16.65 mg g^{-1}. This behavior suggests a rapid diffusion of xylose to the selective sites of the HMIP, favored by the presence of well-defined cavities. In the kinetic study performed, two mathematical models were applied to describe the behavior of xylose adsorption by the synthesized polymers: the pseudo-first-order model and the pseudo-second-order model (Table 2). These models allow us to understand the mechanisms involved in the adsorption process and predict the rate at which xylose is captured by the polymeric materials.

The kinetic models applied to the HMIP and HNIP reveal significant differences in the xylose adsorption mechanisms,

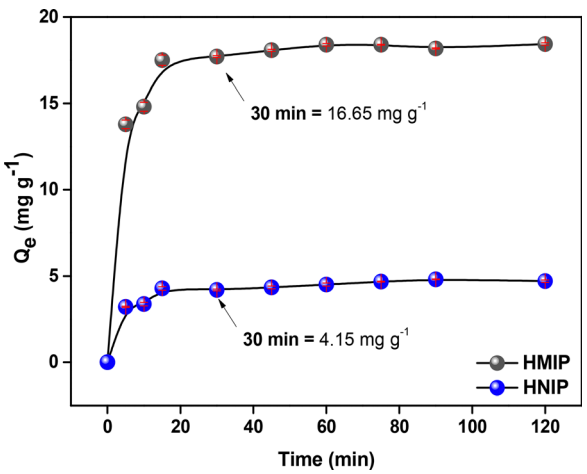

Fig. 5 Kinetic study of xylose adsorption onto the synthesized polymers.

Table 2 Kinetic parameters for the adsorption of xylose onto the HMIP and HNIP

Models	Equation	Polymer	K_1	K_2	Q_e	K_{id}	C	β	α	R^2
Pseudo-first order	$\log(Q_e - Q_t) = \log Q_e - \frac{K_1}{2.303}t$	HMIP	0.26	—	1.85	—	—	—	—	0.79
		HNIP	0.85	—	1.56	—	—	—	—	0.68
Pseudo-second order	$\frac{1}{Q_t} = \frac{1}{K_2 Q_e^2} + \frac{1}{Q_e}t$	HMIP	—	0.04	15.53	—	—	—	—	0.99
		HNIP	—	0.20	4.81	—	—	—	—	0.99
Intraparticle diffusion	$Q_t = C + K_{id}t^{1/2}$	HMIP	—	—	—	0.11	17.28	—	—	0.52
			—	—	—	2.21	8.54	—	—	0.79
		HNIP	—	—	—	0.09	3.71	—	—	0.84
			—	—	—	0.88	0.81	—	—	0.98
Elovich	$Q_t = \frac{1}{\beta}\ln(\alpha\beta) + \frac{1}{\beta}\ln t$	HMIP	—	—	—	—	—	2.14	1.27×10^{15}	0.69
			—	—	—	—	—	0.315	13.99	0.61
		HNIP	—	—	—	—	—	2.56	1588.96	0.90
			—	—	—	—	—	0.77	1.70	0.95

Q_e = adsorption capacity at equilibrium (mg g^{-1}); Q_t = amount adsorbed at time t (mg g^{-1}); K_1 = rate constant of the pseudo-first order model (min^{-1}); K_2 = rate constant of the pseudo-second order model (g mg^{-1} min^{-1}); K_{id} = rate constant of the intraparticle diffusion model (mg g^{-1} $min^{-1/2}$); C = constant associated with the boundary layer in the intraparticle diffusion model (mg g^{-1}); α = initial adsorption rate in the Elovich model (mg g^{-1} min^{-1}); β = parameter related to the activation energy in the Elovich model (mg g^{-1}).

highlighting the selectivity of the molecularly imprinted polymer.

In the pseudo-first order model, the HMIP presented a lower kinetic constant (K_1 = 0.26 min^{-1}) compared to the HNIP (K_1 = 0.85 min^{-1}), indicating a more controlled and selective adsorption, while HNIP adsorbs faster, but nonspecifically. The equilibrium adsorption capacity (Q_e) of the HMIP (1.85 mg g^{-1}) was slightly higher than that of the HNIP (1.56 mg g^{-1}), and the coefficient of determination (R^2) of the HMIP (0.79) was also higher than that of the HNIP (0.68), suggesting that the model describes better the adsorption of the imprinted material. However, since the R^2 values are not high, this model does not represent perfectly the process, with the pseudo-second order model being more appropriate. In fact, in the pseudo-second-order model, both HMIP and HNIP presented an excellent fit (R^2 = 0.99), confirming that this model describes better the adsorption. The HMIP demonstrated a significantly higher adsorption capacity (Q_e = 15.43 mg g^{-1}) compared to the HNIP (Q_e = 4.81 mg g^{-1}), evidencing the presence of selective cavities in the printed material, corroborating the values found experimentally (23.86 mg g^{-1} for the HMIP and 4.15 mg g^{-1} for the HNIP).

However, the HNIP presented a higher value for K_2 (0.20 g mg^{-1}) compared to the HMIP (0.04), indicating that the initial adsorption rate was faster in the non-imprinted polymer, but without resulting in efficient adsorption at equilibrium. This behavior can be attributed to the absence of specific sites in HNIPs, which depend on nonspecific interactions and, therefore, quickly reach a lower adsorption limit.[25,26] In the intraparticle diffusion model, which evaluates the influence of analyte diffusion inside the polymer pores, the HMIP presented higher K_{id} values (0.11 and 2.21 mg g^{-1} $min^{-0.5}$) compared to the HNIP (0.09 and 0.88 mg g^{-1} $min^{-0.5}$), indicating more efficient diffusion in the printed material. However, the higher C values in the HMIP (17.28 and 8.54 mg g^{-1}) suggest that adsorption occurs largely on the surface before diffusion into the polymer, while in the HNIP (C = 3.71 and 0.81) adsorption is more dependent on diffusion. The model fit was better for the HNIP (R^2 = 0.84 and 0.98) than for the HMIP (R^2 = 0.52 and 0.79), reinforcing that in the printed material adsorption is not limited only to intraparticle diffusion, but also involves specific interactions with selective sites. In the Elovich model, which describes chemical adsorption processes on heterogeneous surfaces, the HMIP presented an extremely high α value (1.27×10^{15} and 13.99 mg g^{-1} min^{-1}), indicating a very fast initial adsorption, followed by a deceleration due to the progressive occupation of selective sites. The HNIP, on the other hand, presented much lower α values (1588.96 and 1.70), indicating a less intense and more gradual process. The β values, which indicate the resistance to adsorption, were lower for the HMIP (2.11 and 0.31) than for the HNIP (2.56 and 0.77), suggesting that adsorption was more efficient on the printed material. However, the R^2 coefficients of the Elovich model were significantly higher for the HNIP (0.90 and 0.95) than for the HMIP (0.69 and 0.61), indicating that this model describes better the kinetics of the HNIP, while adsorption on the HMIP follows more complex mechanisms.[27]

In general, the results indicate that adsorption on the HMIP is more selective and efficient, with greater adsorption capacity and less dependence on intraparticle diffusion. The pseudo-second-order model presented the best fit for both polymers, confirming that adsorption occurs by specific chemical interactions on the HMIP, while adsorption on the HNIP is more influenced by diffusion and nonspecific interactions. Thus, the data reinforce that molecular imprinting significantly increases the selectivity and efficiency of the material for xylose adsorption.

The adsorption isotherm results demonstrated that the adsorptive capacity of the HMIP was significantly higher than that of the HNIP (Fig. 6), confirming the presence of selective cavities for xylose. The analyses revealed that the adsorption increased proportionally to the initial concentration of the analyte in the solution until reaching a plateau, indicating the saturation of the adsorption sites in the HMIP. This behavior suggests that the selective sites of the polymer have a limited number of available active sites, which, when occupied, limit the additional adsorption of the analyte.

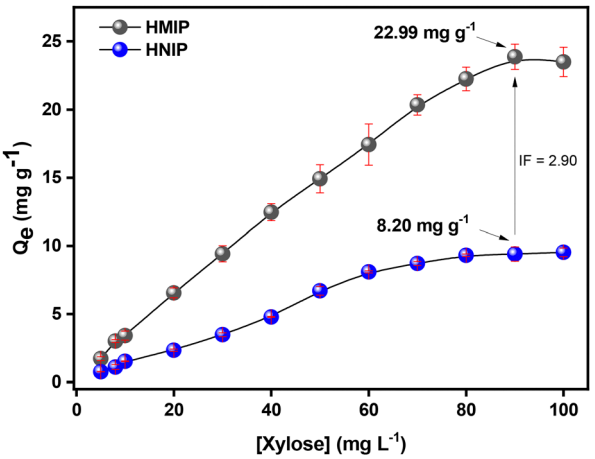

Fig. 6 Adsorption isotherm of xylose onto the HMIP and HNIP using a concentration range of 5 to 100 mg L^{-1}. The HMIP exhibits a significantly higher adsorption capacity compared to the HNIP, confirming the presence of selective binding sites.

Table 3 presents the parameters obtained from the application of four adsorption linear isotherm models (Langmuir, Freundlich, Scatchard and Dubinin–Radushkevich) to compare the performance of the HMIP and HNIP. The Langmuir model considers adsorption on homogeneous surfaces, assuming that all adsorption sites are equivalent and that there is no interaction between the adsorbed molecules.

The results obtained for HMIPs indicated an excellent fit to the model, suggesting the presence of specific and well-organized adsorption sites. In contrast, HNIPs presented behavior incompatible with the model assumptions, evidenced by incoherent parameters and lack of correlation, which indicates the non-existence of specific adsorption sites in this type of material.[28] The Freundlich model, in turn, describes adsorption on heterogeneous surfaces, with different interaction energies. HMIPs presented parameters that indicate favorable and efficient adsorption, with a good fit to the model, which reinforces the presence of active sites with varied affinities. HNIPs, on the other hand, demonstrated lower adsorption efficiency and a surface with less heterogeneity, reflected in lower parameters and a worse fit in relation to HMIPs.[29] The Scatchard model, used to evaluate the affinity and distribution of adsorption sites, revealed that HMIPs have sites with high affinity, with a moderate fit to the model. This confirms the existence of selective interactions in the material. On the other hand, HNIPs presented very low parameters and absence of correlation, indicating the inadequacy of the model due to the lack of selective sites.[30] Finally, the Dubinin-Radushkevich model allows differentiation between physical and chemical adsorption mechanisms based on the average adsorption energy. The results showed that both materials predominantly perform physical adsorption. However, HMIPs presented a superior adsorption capacity and a better fit to the model, with a maximum capacity (Q_m) of 27.55 mg g^{-1} of adsorption, approaching the value found experimentally, evidencing greater efficiency, attributed to the printed structure and the presence of specific cavities. On the other hand, HNIPs, although they also exhibit physical adsorption, demonstrated inferior performance in terms of capacity and correlation.[29]

In summary, the results demonstrate that HMIPs have a significantly higher adsorption capacity and higher affinity compared to HNIPs, as evidenced by the parameters of the Langmuir, Freundlich, Scatchard and Dubinin–Radushkevich models. The consistency of the R^2 values for HMIPs confirms the adequacy of these models, while HNIPs show inconsistencies, especially in the Langmuir and Scatchard models, due to the absence of specific adsorption sites. These data reinforce the effectiveness of molecular imprinting in creating materials with superior adsorption properties.

The non-linear isotherm models (Table S1, ESI†) applied to the HMIP and HNIP show significant differences in xylose adsorption. In the nonlinear Langmuir model, it is observed that the HNIP presents a higher equilibrium constant (K_1), indicating a higher initial affinity for the adsorbate. However, the maximum adsorption capacity (b_1) is higher in the HMIP, confirming that the imprinted polymer has more specific sites for xylose. The coefficient of determination (R^2) suggests a moderate fit for both materials, indicating that this model may not be ideal to fully describe the adsorption. The nonlinear Freundlich model, which considers heterogeneous surfaces, reveals that the MIP presents a higher n exponent than the HNIP, indicating that adsorption is more favorable in this material. Furthermore, the K_1 constant is higher in the HNIP, suggesting that it can adsorb xylose more easily initially, but

Table 3 Parameters of the adsorption isotherm models obtained from the linear fit of the adsorption models

Models	Equation	Polymer	Q_m	K_L	K_F	K_A	K_D	n	ε	R^2
Langmuir	$\frac{C_e}{Q_e} = \frac{1}{Q_m K_L} + \frac{C_e}{Q_m}$	HMIP	34.72	0.06	—	—	—	—	—	0.96
		HNIP	108.45	0.00	—	—	—	—	—	−0.08
Freundlich	$\log Q_e = \log K_F \frac{1}{n} \log C_e$	HMIP	—	—	2.36	—	—	1.43	—	0.96
		HNIP	—	—	0.18	—	—	1.10	—	0.92
Scatchard	$\frac{Q_e}{C_e} = K_A(Q_m - Q_e)$	HMIP	35.41	—	—	0.06	—	—	—	0.82
		HNIP	62.79	—	—	0.00	—	—	—	−0.06
Dubinin–Radushkevich	$\ln Q_e = \ln Q_m - K_D \varepsilon^2$	HMIP	27.55	—	—	—	2.11×10^{-8}		1.54	0.97
		HNIP	8.09	—	—	—	4.55×10^{-8}		1.05	0.85

Q_m = maximum adsorption capacity (mg g^{-1}); K_L = Langmuir's constant (L mg^{-1}); K_F = Freundlich's constant (g mg^{-1}); n = intensity of adsorption (Freundlich); K_A = affinity constant (Scatchard) (L mg^{-1}); K_D = Dubinin–Radushkevich constant (mol^2 kJ^{-2}); ε = mean energy of adsorption (Dubinin–Radushkevich) (kJ mol^{-1}).

without the specificity observed in the case of HMIP. Since R^2 remains similar to that of the Langmuir model, this model also does not fully capture the structural differences between the polymers. In the Langmuir–Freundlich model with one sorption site, which combines features of the Langmuir and Freundlich models, the HMIP has a higher total adsorption capacity (b_1), while the HNIP exhibits a negative exponent n_1, suggesting a less favorable adsorption behavior. R^2 is similar to the previous models, but the lower sum of squared errors (SSE) for the NIP suggests that this model may represent better its adsorption.[31]

The Langmuir–Freundlich model with two sorption sites provides a superior fit, especially for the NIP, with an R^2 = 0.80, indicating that the HNIP has distinct adsorption sites. In the HMIP, this model also fits well, suggesting that despite the selectivity of molecular imprinting, there are still different types of active sites. The higher K_1 value in the HMIP indicates that it contains highly selective sites for xylose, while the HNIP presents a more diffuse adsorption, with higher values of b_1 and b_2, indicating a less controlled distribution of adsorption sites.[26]

In summary, the nonlinear models demonstrate that the HMIP presents a higher adsorption capacity and selectivity for xylose, while the HNIP has a higher initial affinity but lower retention at equilibrium. The two-site sorption model fits the HNIP better, while the one-site model still describes the HMIP well. Compared with the linear models, it is observed that the nonlinear fits provide a more accurate description, especially in the HMIP, where the adsorption heterogeneity is more evident.

3.4. Study of selectivity and interferents

Table 4 presents the selectivity parameters of the molecularly imprinted polymer (HMIP) and the non-imprinted polymer (HNIP) in the adsorption of xylose, compared to the interfering sugars (glucose, fructose, sucrose and arabinose), evaluated separately.

The K_d (distribution coefficient) values indicate the polymer's affinity for the analyte in solution. The HMIP shows higher K_d values than the HNIP, indicating that molecular imprinting enhances xylose selectivity. The selectivity factors (k) compare the adsorption of xylose in relation to the interferents, while the k' values represent the ratio of the selectivity factors between HMIP and HNIP. Higher k' values confirm that the HMIP presents a significantly higher selectivity for xylose in relation to the HNIP. In summary, the results demonstrate that the molecular imprinting process was effective in creating specific binding sites for xylose, ensuring greater selectivity of the HMIP, while the HNIP has a lower capacity to distinguish between analytes. The comparison between the adsorption capacity and the imprinting factor (IF) and the selectivity factor (k') reveals the efficiency of the HMIP in the selective capture of xylose in comparison to competing sugars. The imprinted polymer showed significantly higher adsorption capacity (23.86 mg g^{-1}) when compared to the non-imprinted polymer (8.20 mg g^{-1}), directly reflecting on the calculated imprinting factor (IF = 2.90), which demonstrates the effectiveness of the selective sites formed. The selectivity tests, performed in the presence of glucose, fructose, arabinose and sucrose, showed that the HMIP maintained high affinity for xylose, with selectivity factors (k') ranging from 2.25 to 8.09, depending on the interferent considered. These values are in line with the selectivity coefficients (k and k') obtained (Table 4), which reinforce that the HMIP has a remarkable ability to distinguish xylose from other monosaccharides, even in binary or complex systems. The value of k' = 8.09 for the xylose/glucose pair, for example, indicates that the affinity of the HMIP for xylose is more than eight times greater than for glucose under the same conditions, which highlights its selective robustness.

Table 4 Selectivity parameters of the imprinted (HMIP) and non-imprinted (HNIP) polymer for xylose adsorption compared to interfering sugars

		K_d			
Sugars	Polymers	HMIP	HNIP	k	k'
Xylose/glucose	HMIP	8.98	10.11	0.89	8.09
	HNIP	1.14	10.02	0.11	
Xylose/fructose	HMIP	8.94	10.95	0.82	5.46
	HNIP	1.38	9.40	0.15	
Xylose/sucrose	HMIP	9.35	13.60	0.69	3.13
	HNIP	1.75	8.03	0.22	
Xylose/arabinose	HMIP	9.35	15.27	0.61	2.25
	HNIP	1.75	6.54	0.27	

As illustrated in Fig. 7, the study of the interferents presented promising results, evidencing that the HMIP exhibited consistently superior adsorptive performance to the HNIP in all binary analysis performed at a concentration of 50 mg L^{-1}. Although xylose was the least adsorbed compound among the sugars tested, the HMIP demonstrated high selectivity not only for xylose, but also for glucose, fructose and sucrose, reinforcing its efficiency even in the presence of possible interferents. Among the systems evaluated, sucrose was the interferent with the greatest impact; however, the HMIP remained more efficient than the HNIP in all cases. The results indicate that the presence of glucose, fructose, and sucrose significantly interferes with xylose adsorption, reducing its Q_e value. This reduction can be attributed to the structural similarity between the sugars, especially the presence of $-CH_2OH$ groups and multiple hydroxyls, which favor the formation of hydrogen bonds with the HMIP, competing for the active sites. Despite this, HMIP showed superior performance to HNIP, highlighting the relevance of the imprinted selective sites for xylose adsorption, even in the presence of interferents. Furthermore, the interaction of the HMIP with different monosaccharides suggests its potential not only for the selective purification of xylose, but also for broader applications, such as the separation and detection of carbohydrates in complex matrices. This opens promising perspectives for the use of the material in industrial processes, such as biomass refining, food production, and development of analytical sensors.

Borges *et al.* developed a MIP using precipitation polymerization and non-covalent interactions for xylose extraction.[5] In contrast, the present study presented a more comprehensive

Table 5 Comparative table with recent studies (2023–2025) on carbohydrate-selective hollow MIPs

MIP	Analyte	Extraction method	Adsorptive capacity (mg g^{-1})	Impression factor	Samples	Ref.
MIP	Fructose	DSPE	7.20	1.47	—	32
MIP	Lactose	DSPE	14.00	4.70	Aqueous solution	33
MIP	Glucose	Heat transfer method	2.81	5.18	Human urine	33
MIP	Galactose	DSPE	144.00	—	—	34
MIP	Reveratrol	DSPE	10.00	16.00	*Polygonum cuspidatum*	35
HMIP	Xylose	DSPE	22.99	2.90	Sugarcane	This work

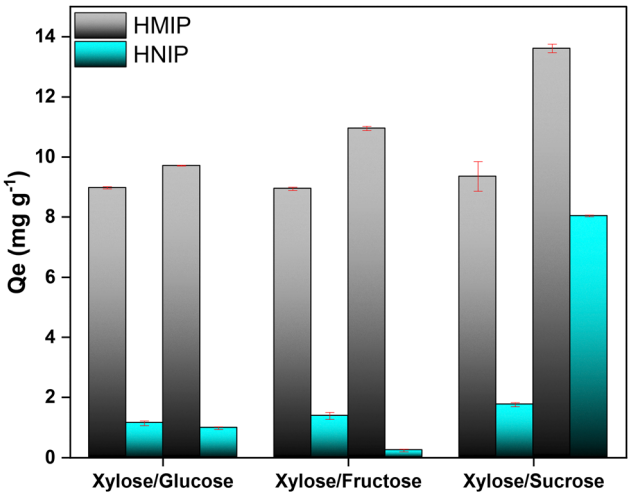

Fig. 7 Equilibrium adsorption capacity (Q_e) of the imprinted (HMIP) and non-imprinted (HNIP) polymer for xylose in the presence of different interferents (glucose, fructose and sucrose) in binary mixtures.

evaluation of the interferents, with the results more representative of the reality of complex samples. The developed HMIP demonstrated a significantly higher adsorptive capacity for xylose (23.86 mg g^{-1}) compared to the MIP of Borges *et al.* (11.48 mg g^{-1}), evidencing its greater efficiency. An important differential of this work was the performance of tests with binary mixtures of xylose with other sugars (glucose, fructose and sucrose), which allowed evaluating the behavior of the polymer against simultaneous interferences, as it occurs in real matrices. Even with a slight reduction in xylose adsorption—especially in the presence of sucrose—the HMIP maintained superior performance to the HNIP, demonstrating selectivity and robustness in more complex systems. On the other hand, although the MIP proposed by Borges showed high selectivity for xylose in individual tests, it was not evaluated in binary or complex systems, which represents a limitation to predict its performance in real matrices, in which there is competition between analytes. Thus, the results obtained in this study reinforce the importance of simultaneous analysis in the validation of selective materials for practical applications.

Table 5 presents some studies with hollow porous MIPs, and some parameters defined by them, for comparison purposes. To evaluate the performance of the hollow molecularly imprinted porous polymer (HMIP) developed in this study, the table presents a comparative overview of recent works involving carbohydrate-selective MIPs. Although the HMIP developed in this study showed lower adsorption capacity when compared to certain materials reported in the literature, this behavior is attributed to its hollow porous architecture. This structural design, while providing a thinner polymeric layer and lower total mass per particle, significantly improves mass transfer and accessibility to recognition sites. As a result, despite the moderate adsorption capacity (22.99 mg g^{-1}), the HMIP maintained high selectivity for D-xylose, as confirmed by the imprinting factor (2.90) and the performance in real lignocellulosic matrices. Furthermore, the material developed in this work presents distinct advantages compared to other systems. Unlike several previous studies that focused on model solutions or required extensive synthetic steps, the HMIP here was synthesized using a more environmentally friendly route with reduced solvent consumption and demonstrated excellent reusability, maintaining over 80% efficiency after ten cycles. Furthermore, its effective integration into the dispersive solid-phase extraction (DSPE) workflow, combined with filtration steps, allowed the mitigation of interferents such as phenolics and organic acids, improving analytical performance in complex biomass hydrolysates. Overall, the developed HMIP stands out not only for its selectivity and practical applicability, but also for its alignment with sustainable analytical practices and its robustness under real sample conditions.

3.5. Determination of xylose in sugarcane samples by HPLC-IR and its extraction by the DSPE method

Initially, the hydrolyzed sugarcane bagasse sample was analyzed by HPLC-IR to determine the actual xylose concentration. The data in Table 6 show that the sample has a high concentration of xylose and a reduced amount of interferents, such as glucose and arabinose. To optimize this process, the sample was diluted in acetonitrile before application in DSPE, ensuring better conditions for HMIP selectivity.

In the extraction of xylose using the DSPE method, SPE analysis was performed for comparative purposes. The comparison between the results of SPE and DSPE revealed significant differences in the adsorption efficiency of xylose (Table 7). In the SPE method, the adsorption was more selective, but the recovery of the analyte was lower due to the longer contact time and possible irreversible retention in the polymer sites. In the DSPE method, the dispersion of the adsorbent in the solution favored a more efficient interaction between xylose and the selective sites of the HMIP, resulting in greater recovery of the analyte and less interference from other sugars. Thus, DSPE proved to be a faster and more efficient method for the extraction of xylose, providing a balance between selectivity and recovery of the analyte in the analyzed matrix.

The reuse of the HMIP was evaluated through successive cycles of xylose adsorption and desorption, using acetonitrile

Table 6 Evaluation of sugar concentrations in hydrolyzed sugarcane bagasse samples by HPLC-RI

Monosaccharide	Concentration (g L^{-1})
Xylose	26.29 ± 0.15
Glucose	3.79 ± 0.05
Arabinose	3.58 ± 0.04

n = 3.

Table 7 Xylose extraction using HMIP and HNIP by SPE and DSPE. Xylose concentration: 26.29 g L^{-1}

Extraction method	% Extraction		Xylose concentration (g L^{-1})	
	HMIP	HNIP	HMIP	HNIP
SPE	83.80 ± 2.40	44.33 ± 0.72	22.04 ± 0.63	11.66 ± 0.18
DSPE	98.74 ± 0.11	64.91 ± 1.43	25.97 ± 0.02	17.07 ± 0.37

n = 3.

(ACN) for material regeneration. The results showed that, in the first cycle, the xylose recovery rate was approximately 94%, maintaining high values in the first five cycles. After the fifth cycle, there was a slight decrease in efficiency, reaching 87% in the sixth cycle and 81% in the tenth cycle, indicating a progressive reduction in the adsorption capacity. Despite this decrease, the HMIP demonstrated good stability and reuse potential, making the process more economical and sustainable for future applications.

Furthermore, mitigation of typical interferents in lignocellulosic hydrolysates—including phenolic compounds, organic acids (*e.g.*, acetic acid, formic acid), and salts—was achieved by combining DSPE using HMIP and filtration prior to HPLC analysis. The DSPE step effectively reduced carbohydrate-related interferents, while filtration removed most hydrophobic compounds, such as lignin-derived phenolics, which are known to co-elute or suppress signals in IR detection. This two-step cleanup significantly improved baseline stability and peak resolution in the chromatograms.

4. Conclusion

The present study highlights the potential of the molecularly imprinted polymer (HMIP) in the selective adsorption of xylose in complex media, indicating its applicability in the separation and purification of monosaccharides. Based on the overall analysis, the HMIP emerges as a promising alternative for the selective separation of xylose, with possible applications in biomass purification, industrial process control, and analytical methods for carbohydrate detection. Future studies may focus on structural modifications of the polymer to further enhance its selectivity and efficiency in complex systems. In addition to its technical advantages, the synthesis route adopted for the HMIP presented relevant environmental benefits. The process led to a reduction of approximately 35% in solvent consumption and energy demand, with an estimated environmental factor (E-factor) of 230 kg of waste per kg of product---significantly lower than the average value of 350 kg kg^{-1} reported for conventional MIPs. These aspects reinforce that the developed strategy not only meets technical efficiency criteria but is also in strong alignment with the principles of sustainable chemistry and the objectives of SDG 12, promoting a cleaner, more efficient, and environmentally responsible production model.

Author contributions

Diogo Hideki Moriya: methodology, validation, and investigation. Cláudio Fernando de Souza Teles: validation and investigation. Paula Mantovani dos Santos: formal analysis and writing – original draft. Ademar Wong: formal analysis and writing – original draft. Maria D. P. T. Satomayor: conceptualization, resource, writing – review and editing, supervision, funding acquisition.

Conflicts of interest

The authors declare that they have no known competing financial interests or personal relationships that could have appeared to influence the work reported in this paper.

Data availability

The data that support the findings of this study are available from the corresponding author [M. D. P. T. Sotomayor] upon reasonable request.

Acknowledgements

The authors are grateful for the collaboration of the National Council for Scientific and Technological Development (CNPq, grant no. 102213/2024-0, 150256/2024-8 and 405916/2023-0), Coordination for the Improvement of Higher Education Personnel (CAPES), and São Paulo State Research Support Foundation (FAPESP grant no. 2023/06494-7 and 2017/20401-8). We thank the LACFI laboratory of the Federal University of Santa Catarina (UFSC) for the BET analyses.

References

1 B. C. Saha, Hemicellulose bioconversion, *J. Ind. Microbiol. Biotechnol.*, 2003, **30**, 279–291.
2 F. H. Isikgor and C. R. Becer, Lignocellulosic biomass: a sustainable platform for the production of bio-based chemicals and polymers, *Polym. Chem.*, 2015, **6**, 4497–4559.
3 L. Uzun and A. P. F. Turner, Molecularly-imprinted polymer sensors: realising their potential, *Biosens. Bioelectron.*, 2016, **76**, 131–144.
4 H. Zhang, Water-compatible molecularly imprinted polymers: Promising synthetic substitutes for biological receptors, *Polymer*, 2014, **55**, 699–714.

5 L. F. T. Borges, A. Wong, W. R. Silva and M. D. P. T. Sotomayor, Development of a Non-Covalent Molecularly Imprinted Polymer via Precipitation Method for the Selective Separation of D-Xylose From Sugarcane Residues, *J. Sep. Sci.*, 2024, **47**, e70024.
6 J. J. BelBruno, Molecularly Imprinted Polymers, *Chem. Rev.*, 2019, **119**, 94–119.
7 S. Orbay, O. Kocaturk, R. Sanyal and A. Sanyal, Molecularly Imprinted Polymer-Coated Inorganic Nanoparticles: Fabrication and Biomedical Applications, *Micromachines*, 2022, **13**, 1464.
8 S. Bhogal, K. Kaur, I. Mohiuddin, S. Kumar, J. Lee, R. J. C. Brown, K.-H. Kim and A. K. Malik, Hollow porous molecularly imprinted polymers as emerging adsorbents, *Environ. Pollut.*, 2021, **288**, 117775.
9 R. R. Pupin and M. D. P. T. Sotomayor, Synthesis and evaluation of hollow porous molecularly imprinted polymer for selective determination of tetracycline, *J. Mater. Sci.*, 2022, **57**, 17291–17303.
10 S. Zhou, J. Fu, P. Zhao, S. Tang, X. Wu, Z. Yang and Z. Zhang, Hollow magnetic molecularly imprinted polymer based on metal-organic framework for capture of ciprofloxacin, *Sep. Sci. plus*, 2022, **5**, 337–348.
11 Y. Hua, V. Kumar and K.-H. Kim, Recent progress on hollow porous molecular imprinted polymers as sorbents of environmental samples, *Microchem. J.*, 2021, **171**, 106848.
12 Y. Zhao, Molecularly imprinted materials for glycan recognition and processing, *J. Mater. Chem. B*, 2022, **10**, 6607–6617.
13 C. Li, Y. Ma, H. Niu and H. Zhang, Hydrophilic Hollow Molecularly Imprinted Polymer Microparticles with Photo- and Thermoresponsive Template Binding and Release Properties in Aqueous Media, *ACS Appl. Mater. Interfaces*, 2015, **7**, 27340–27350.
14 L. C. Cabrera, M. L. Martins, E. G. Primel, O. D. Prestes, M. B. Adaime and R. Zanella, Extração em Fase Sólida Dispersiva na determinação de resíduos e contaminantes em alimentos, *Sci. Chromatogr.*, 2012, **4**, 227–240.
15 R. A. Sheldon, The E Factor: fifteen years on, *Green Chem.*, 2007, **9**, 1273.
16 J. H. Roe and E. W. Rice, A Photometric Method For The Determination Of Free Pentoses In Animal Tissues, *J. Biol. Chem.*, 1948, **173**, 507–512.
17 R. Kumar, M. Tabatabaei, K. Karimi and I. Sárvári Horváth, Recent updates on lignocellulosic biomass derived ethanol - A review, *Biofuel Res. J.*, 2016, **3**, 347–356.
18 A. Sluiter, Determination of Sugars, Byproducts, and Degradation Products in Liquid Fraction Process Samples: Laboratory Analytical Procedure (LAP) Issue Date: 12/08/2006, Technical Report.
19 M. Luna Quinto, S. Khan, J. Vega-Chacón, B. Mortari, A. Wong, M. D. P. Taboada Sotomayor and G. Picasso, Development and Characterization of a Molecularly Imprinted Polymer for the Selective Removal of Brilliant Green Textile Dye from River and Textile Industry Effluents, *Polymers*, 2023, **15**, 3709.
20 H. Yang, S. Nishitani and T. Sakata, Potentiometric Langmuir Isotherm Analysis of Histamine-Selective Molecularly Imprinted Polymer-Based Field-Effect Transistor, *ECS J. Solid State Sci. Technol.*, 2018, **7**, Q3079–Q3082.
21 P. A. G. Cormack and A. Z. Elorza, Molecularly imprinted polymers: synthesis and characterisation, *J. Chromatogr. B:Anal. Technol. Biomed. Life Sci.*, 2004, **804**, 173–182.
22 M. A. Karimi, A. Hatefi-Mehrjardi, S. Z. Mohammadi, A. Mohadesi, M. Mazloum-Ardakani, A. A. Kabir, M. Kazemipour and N. Afsahi, Solid phase extraction of trace amounts of silver(I) using dithizone-immobilized alumina-coated magnetite nanoparticles prior to determination by flame atomic absorption spectrometry, *Int. J. Environ. Anal. Chem.*, 2012, **92**, 1325–1340.
23 V. K. Gupta, S. Agarwal and T. A. Saleh, Chromium removal by combining the magnetic properties of iron oxide with adsorption properties of carbon nanotubes, *Water Res.*, 2011, **45**, 2207–2212.
24 M. C. Wang, L. A. Valenzuela, G. P. Murphy and T. M. Chu, Purification of a Human Prostate Specific Antigen, *J. Urol.*, 1979, **17**, 159–163.
25 Y. S. Ho and G. McKay, Pseudo-second order model for sorption processes, *Process Biochem.*, 1999, **34**, 451–465.
26 P. M. Dos Santos, M. Zanetti Corazza and C. Ricardo Teixeira Tarley, Synthesis of ionically imprinted Poly(Alylthiourea) in the presence of 1-(2-Pyridylazo)-2-Napthol (PAN) for preconcentration in magnetic dispersive solid phase of nickel ions in water and food samples, *Food Chem.*, 2024, **440**, 138238.
27 G. Wulff, Molecular Imprinting in Cross-Linked Materials with the Aid of Molecular Templates— A Way towards Artificial Antibodies, *Angew. Chem., Int. Ed. Engl.*, 1995, **34**, 1812–1832.
28 X. Guo and J. Wang, Comparison of linearization methods for modeling the Langmuir adsorption isotherm, *J. Mol. Liq.*, 2019, **296**, 111850.
29 D. A. O. Langmuir, Freundlich, Temkin and Dubinin–Radushkevich Isotherms Studies of Equilibrium Sorption of Zn^{2+} Unto Phosphoric Acid Modified Rice Husk, *IOSRJAC*, 2012, **3**, 38–45.
30 X. Chen, Modeling of Experimental Adsorption Isotherm Data, *Information*, 2015, **6**, 14–22.
31 G. P. Jeppu and T. P. Clement, A modified Langmuir-Freundlich isotherm model for simulating pH-dependent adsorption effects, *J. Contam. Hydrol.*, 2012, **129–130**, 46–53.
32 A. Xu, E. Rodrigues, P. Sampaio, M. A. Marques, J. Alves and A. M. L. Piloto, Molecularly imprinted polymer fluorescent spots (MIP@spots) for CA 19-9 detection on a solid substrate, *Sens. Int.*, 2025, **6**, 100333.
33 F. Hadizadeh, A. Zakerian and S. A. Mohajeri, Non-covalently lactose imprinted polymers and recognition of saccharides in aqueous solutions, *J. Iran. Chem. Soc.*, 2013, **10**, 207–212.
34 B. Okutucu, S. Önal and A. Telefoncu, Noncovalently galactose imprinted polymer for the recognition of different saccharides, *Talanta*, 2009, **78**, 1190–1193.
35 J. Cao, C. Shen, X. Wang, Y. Zhu, S. Bao, X. Wu and Y. Fu, A porous cellulose-based molecular imprinted polymer for specific recognition and enrichment of resveratrol, *Carbohydr. Polym.*, 2021, **251**, 117026.